INTERFACE FOCUS

rsfs.royalsocietypublishing.org

Research

Cite this article: Liyanage W, Rubeo PW, Nilsson BL. 2017 Redox-sensitive reversible self-assembly of amino acid–naphthalene diimide conjugates. *Interface Focus* **7**: 20160099.
http://dx.doi.org/10.1098/rsfs.2016.0099

One contribution of 12 to a theme issue 'Self-assembled peptides: from nanostructures to bioactivity'.

Subject Areas:
biomaterials, nanotechnology

Keywords:
self-assembly, stimulus-responsive, phenylalanine, naphthalene diimide

Author for correspondence:
Bradley L. Nilsson
e-mail: nilsson@chem.rochester.edu

Electronic supplementary material is available online at https://dx.doi.org/10.6084/m9.figshare.c.3881758.

THE ROYAL SOCIETY PUBLISHING

Redox-sensitive reversible self-assembly of amino acid–naphthalene diimide conjugates

Wathsala Liyanage, Paul W. Rubeo and Bradley L. Nilsson

Department of Chemistry, University of Rochester, Rochester, NY 14627-0216, USA

BLN, 0000-0003-1193-3693

Peptide and low molecular weight amino acid-based materials that self-assemble in response to environmental triggers are highly desirable candidates in forming functional materials with tunable biophysical properties. In this paper, we explore redox-sensitive self-assembly of cationic phenylalanine derivatives conjugated to naphthalene diimide (NDI). Self-assembly of the cationic Phe-NDI conjugates into nanofibrils was induced in aqueous solvent at high ionic strength. Under reducing conditions, these self-assembled Phe-NDI conjugate fibrils underwent a morphological change to non-fibril aggregates. Upon reoxidation, the initially observed fibrils were reformed. The study herein provides an interesting strategy to effect reversible switching of the structure of supramolecular materials that can be applied to the development of sophisticated stimulus-responsive materials.

1. Background

Amyloid-inspired self-assembly of peptides and amino acids into highly ordered fibril assemblies has been exploited for the creation of functional materials [1–8]. The emergent properties of peptide-derived self-assembled materials depend on the molecular structure of the assembly motifs. Covalent [9] or non-covalent [10–12] incorporation of additional functionality into these self-assembling materials is beneficial in forming self-assembly systems with integrated molecular functions. Stimulus-responsive self-assembly is a highly desired function for supramolecular materials [13–17].

Recently, development of short peptide sequences decorated with organic π-systems has emerged as a powerful method to tune the properties of self-assembly [9]. Electron-deficient, aromatic 1,4,5,8-naphthalene diimides (NDIs) with well-defined redox and spectroscopic properties have been widely used in π-conjugate systems to fabricate supramolecular nanomaterials [18–29]. For example, incorporation of an electron-deficient NDI functional module into a β-sheet forming dipeptide resulted in *n*-type one-dimensional nanostructures [30] that can be modified to form self-supporting hydrogels [31]. Ulijn and co-workers [32] have shown that NDI–tyrosine conjugates can be enzymatically combined with Phe-NH_2 to form NDI-YF-NH_2 self-supporting hydrogels. Similarly, Lin *et al.* [33] recently demonstrated that NDI-Phe-Phe and NDI-Phe-Gly conjugates formed coloured hydrogels under both acidic and physiological conditions. More recently, they demonstrated that equimolar ratios of NDI–lysine and NDI–serine conjugates were able to co-assemble into hydrogels under neutral conditions [34]. Bhosale and co-workers also demonstrated the assembly of several NDI–amino acid and dipeptide systems into distinct materials, including golf ball-like nanostructures derived from an NDI–dipeptide [35] as well as nanobelts formed from co-assembly of NDI motifs containing phosphonic acid groups with L- and D-arginine [36].

NDI-grafted peptides have also been found to provide precise stimulus-responsive control in initiating supramolecular self-assembly processes. Ghadiri and co-workers investigated the redox-triggered self-assembly of cyclic peptides with alternating L- and D-amino acid sequences in which NDI derivatives were appended to Lys side chains [37]. They found that these cyclic peptides assembled into D, L-α-peptide nanotubes upon reduction of the attached NDI side chain

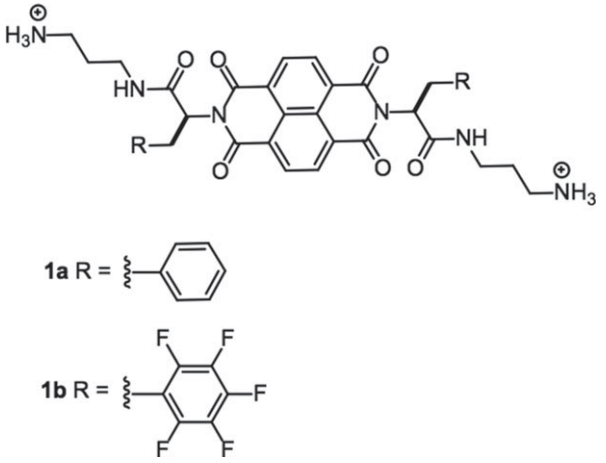

Figure 1. Chemical structures of NDI-Phe conjugates used in these studies.

groups. This demonstration of reduction-triggered self-assembly highlights the interesting potential of NDI to influence the supramolecular self-assembly behaviour of NDI conjugates. Examples of supramolecular systems that can reversibly assemble/disassemble or switch between different emergent morphologies in response to stimuli are more rare. We reasoned that the redox potential of NDI makes it an attractive moiety to develop materials that can exhibit altered properties under oxidizing or reducing conditions and that these properties may be switchable as a function of repeated alteration of the redox environment.

As such, we sought to demonstrate that NDI conjugates could be used to reversibly alter supramolecular material properties in a stimulus-responsive manner. Fluorenylmethoxycarbonyl-Phe (Fmoc-Phe) and side chain modified derivatives of Fmoc-Phe are privileged supramolecular self-assembly motifs [38–42]. We reasoned that NDI may be an effective proxy of the Fmoc-group, and that NDI-Phe conjugates may undergo effective self-assembly into fibrils in which redox environment may influence the nature of the supramolecular materials. We thus synthesized symmetrical, NDI–phenylalanine (NDI-Phe) conjugates **1a** and **1b** (figure 1). We have previously shown in the context of Fmoc-Phe self-assembly, that pentafluorophenylalanine (F_5-Phe) has enhanced self-assembly propensity relative to Phe [43]. Thus, both Phe (**1a**) and F_5-Phe (**1b**) NDI conjugates were prepared. The cationic appendages to the Phe-derivative termini were used to enhance the water solubility of these conjugates. It was found that these NDI-Phe conjugates self-assembled into one-dimensional fibrils in aqueous solutions with high ionic strength. Upon reduction, the resulting anionic species affected a conformational rearrangement of the supramolecular fibrils to amorphous aggregates. Upon reoxidation, the fibril morphology was restored. This process was reversible and the cycle could be repeated with the same results each time. Detailed below is a discussion of these findings that elucidate the interesting potential for NDI to be used to alter the emergent properties of supramolecular materials.

2. Material and methods

2.1. Synthesis

The synthesis of NDI congeners **1a** and **1b** is shown in scheme 1 and described in detail in the electronic supplementary material. These analogues were prepared by a modification to a published NDI conjugation protocol [44]. Briefly, 1,4,5,8-naphthalenetetracarboxylic dianhydride in dimethylformamide was condensed with Phe derivatives to obtain diimide functionalized compounds **2a** and **2b**. *Tert*-butyl-(3-aminopropyl)carbamate moieties were appended at the C-termini of these Phe derivatives to yield **3a** and **3b**. Trifluoroacetic acid-mediated deprotection of *N*-Boc residues then afforded **1a** and **1b**. Characterization data, including NMR and mass spectroscopy analysis can be found in electronic supplementary material, figures S1–S14.

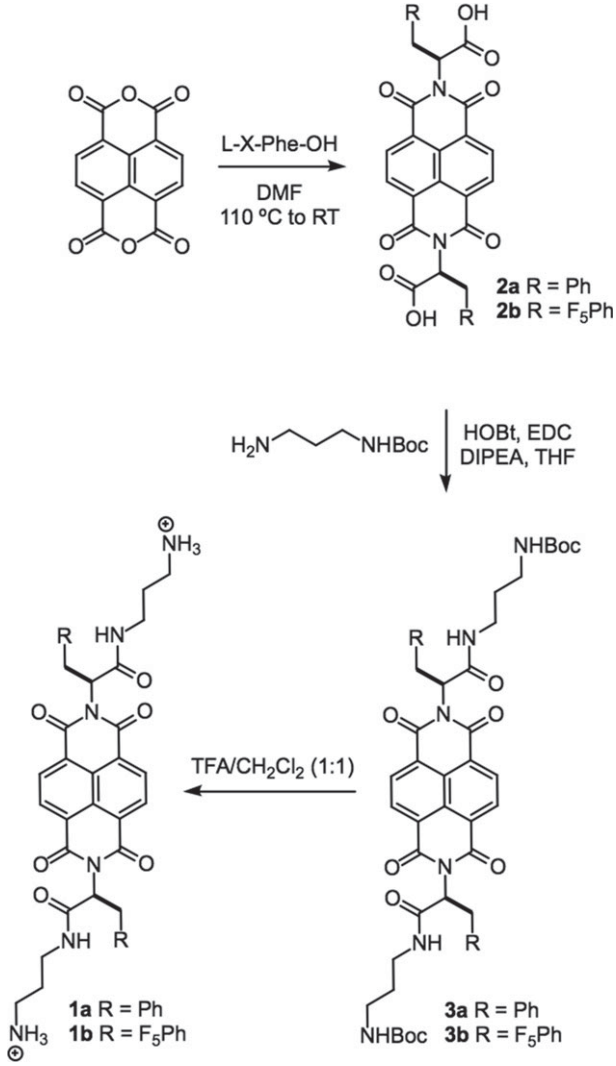

Scheme 1. Synthesis of NDI-Phe conjugates.

2.2. Self-assembly

Self-assembly was initiated by dissolving **1a** or **1b** in unbuffered filtered water (Barnstead NANOpure 0.2 µm filter, 18 Ω) to obtain NDI-Phe conjugate stock solutions (10 mM). Stock NDI-Phe conjugate solutions were then diluted to 5 mM in aqueous brine solutions (100–1000 mM NaCl).

2.3. Circular dichroism spectroscopy

Circular dichroism (CD) spectra were recorded on an AVIV 202 CD spectrometer. NDI-Phe conjugate samples (5 mM) were analysed immediately after dilution into 100–1000 mM NaCl. Spectra were obtained from 300 to 190 nm with a 1.0 nm step, 1.0 nm bandwidth and a 6 s collection time per step at 25°C in a 0.1 mm path length quartz cuvette (Hellma). The AVIV software was used for background subtraction, conversion to molar ellipticity and data smoothing with a least-squares fit.

2.4. Transmission electron microscopy

Images were obtained with a Hitachi 7650 transmission electron microscope with an accelerating voltage of 80 kV. Freshly prepared

samples (10 µl) were spotted onto 200 mesh carbon-coated copper grids and allowed to stand for 1 min. Excess sample was carefully removed by capillary action using filter paper and then grids were immediately stained with uranyl acetate negative stain (10 µl for 2 min). Excess stain was removed by capillary action and grids were allowed to air-dry for 10–15 min. Dimensions of nanostructures were determined using ImageJ64 software.

2.5. Scanning electron microscopy

Images were taken on a Zeiss Supra 40VP FESEM scanning electron microscope with 10 kV accelerating voltage. Samples were placed on glass plates and excess solvent was removed by capillary action (filter paper). Then the air-dried samples were sputter coated with gold at a 1 $\mathring{A}\ s^{-1}$ rate using low vacuum sputter-coating system under 100 mTorr pressure in 15 mA current.

2.6. UV–visible and fluorescence spectroscopy

UV spectra were collected using a TECAN Infinite plate reader fluorimeter from 230–800 nm and background was subtracted. Spectra of each NDI-Phe conjugate sample were obtained from 200 µM samples in H_2O. The reduced NDI-Phe conjugate samples were prepared by diluting NDI-Phe conjugate stock solutions into aqueous 50 mM $Na_2S_2O_4$.

2.7. Cyclic voltammetry

Cyclic voltammetry (CV) measurements of the NDI-Phe conjugate samples (1 M) were performed with a CHI 680D potentiostat using a glassy-carbon working electrode, a glassy-carbon auxiliary electrode and SCE reference electrode. The CV was recorded for 0.5 mM **1a** or **1b** in the presence of 0.1 M $TBAPF_6$ in a 1/1 acetonitrile/H_2O mixture at room temperature with a $mM\ s^{-1}$ scan rate. The instrument was purged with argon 10 min before performing a CV experiment. Under these solvent conditions no assembly was observed, indicating that the observed redox potentials are independent of the assembly properties of the NDI-Phe and NDI-F_5-Phe conjugates.

2.8. Electron paramagnetic resonance studies

Electron paramagnetic resonance (EPR) spectra were obtained with a Bruker X-band EPR spectrometer model EMXplus operating at approximately 9.8 GHz microwave frequency with a high 100 kHz magnetic field modulation frequency at 298 K. A standard EPR cavity was used and the microwave power was kept to a minimum to avoid saturating the radical spins. The magnetic fields and *g*-values were calibrated with a standard solid powder sample of diphenyl picryl hydrazyl ($g = 2.0036$). The EPR of the blank quartz tube was measured to calibrate EPR baseline for the samples. Quartz AquaX EPR tubes were used. The quartz EPR tubes were washed thoroughly with distilled and deionized water and dried before each use. Samples were prepared at concentrations of 5 mM NDI-Phe with 1 M NaCl and 50 mM $Na_2S_2O_3$.

3. Results and discussion

3.1. Self-assembly of NDI-Phe conjugates

We initially attempted to study the aqueous self-assembly of the **2a** and **2b** carboxylic acid derivatives, but the poor water solubility of these molecules was limiting. To circumvent the poor water solubility of **2a** and **2b**, *tert*-butyl-(3-aminopropyl) amine was coupled to the C-termini of the Phe derivatives of **2a** and **2b** to provide amides **3a** and **3b**. Deprotection of the Boc-amine group gave amines **1a** and **1b**. Compounds **1a** and **1b** exhibited dramatically improved water solubility.

While other amino acid–NDI conjugates have been previously shown to self-assemble [34], compounds **1a** and **1b** failed to self-assemble in simple aqueous solutions. The amine cations of these molecules that impart water solubility also introduce repulsive charge effects that impede intermolecular interactions. Other cationic self-assembling peptide systems have been shown to undergo self-assembly at high ionic strength in solutions with high salt concentrations [16,45]. At high salt concentrations cationic charges can be shielded and repulsive effects are minimized.

Accordingly, we assessed the self-assembly behaviour of **1a** and **1b** in the presence of increasing concentrations of NaCl. Compounds **1a** and **1b** were dissolved in unbuffered water (18 Ω) to obtain homogeneous NDI-Phe conjugate solutions, which were diluted into aqueous brine solutions (5 mM NDI-Phe derivative) with NaCl concentrations ranging from 100 to 1000 mM. The least hydrophobic Phe-NDI conjugate **1a** showed no evidence of self-assembly as evidenced by extensive transmission electron microscopy (TEM) analysis even after increasing NaCl concentration to 1000 mM. However, the more hydrophobic F_5-Phe-NDI compound **1b** effectively self-assembled into rigid fibrils over a range of NaCl concentrations (100–1000 mM; figure 2). The fibril solutions were optically transparent, indicating that the assembled fibrils remained in a solvated state after assembly. At 100 mM NaCl, **1b** formed fibrils of 12 ± 2 nm in diameter (figure 2*a*). As solvent ionic strength increased, wider fibrils ranging from 20 to 30 nm in diameter formed through the apparent bundling of the smaller 12 nm fibrils (figure 2*b*,*c*). The influence of ionic strength on the self-assembled structure of **1b** was also assessed by CD spectroscopy. The CD spectrum of **1b** showed a distinctive minimum at 221 nm, a maximum at 194 nm, with a crossover at 205 nm (figure 2*d*). The intensity of the CD signal increased as the solvent ionic strength increased, reaching a maximum intensity at approximately 500 mM NaCl. These data are consistent with an increased propensity towards self-assembly as solution ionic strength is increased, similar to observations from self-assembling peptide systems [45]. The failure of compound **1a** to self-assemble can be attributed to the much lower hydrophobicity of Phe relative to the F_5-Phe groups found in compound **1b**.

3.2. Influence of redox environment on self-assembly

The effect of redox environment on the self-assembled fibrils of **1b** was next explored. The addition of aqueous sodium dithionite ($Na_2S_2O_4$, 50 mM), a mild chemical reductant, to self-assembled **1b** fibrils resulted in an immediate conversion from fibril to spherical/amorphous aggregates as evidenced by TEM images (figure 3*b*). The reduced **1b** aggregates were globular in appearance, with diameters of approximately 100–200 nm. Also, the optically transparent solutions of the self-assembled fibrils become turbid upon addition of reductant. Upon air oxidation, the globular aggregates begin to convert into protofibril species that eventually (over 16 h) completely revert back to the originally observed supramolecular fibrils (figure 3*b*–*f*). The transient protofibril intermediates observed during the NDI radical quenching process provide interesting insight into the self-assembly process, providing a glimpse of possible early aggregates formed during **1b** fibril assembly. It is also significant that repeated addition of sodium dithionite followed by a period of reoxidation in ambient oxygen causes this morphological conversion to occur in a

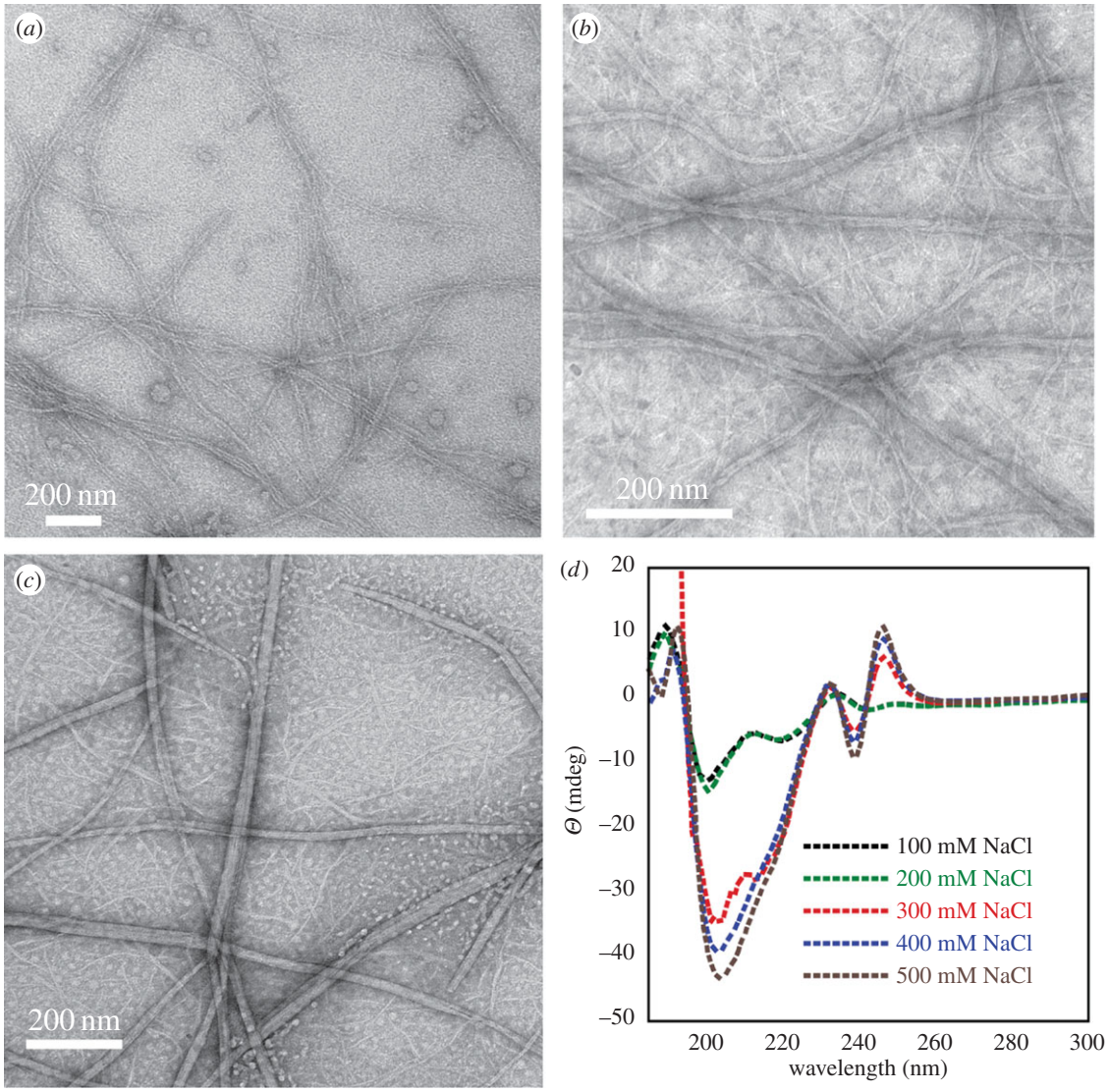

Figure 2. TEM images of fibrils of **1b** (5 mM) in aqueous solutions with varying concentrations of NaCl: (*a*) 100 mM NaCl, (*b*) 500 mM NaCl and (*c*) 1000 mM NaCl. (*d*) CD spectra of fibrils of **1b** (5 mM) at varying concentrations of NaCl. The decreased signal intensity at 194 nm is an artefact of increased dynode voltage in the spectrometer from high salt concentrations, which obscures signals in the far-UV.

repeatable manner. This is a significant demonstration of reversible switching from one supramolecular aggregate to another, showing the great potential of NDI conjugates to be used in the design of dynamic supramolecular materials.

Interestingly, our morphological transition from fibrils under oxidizing conditions to globular aggregates under reducing conditions differs from previously observed reduction-triggered assembly of NDI-bearing cyclic peptides. As described in the Introduction, Ghadiri and co-workers [37] previously showed that cyclic D/L-peptides undergo selective *assembly* under reducing conditions. This was explained based on the assumption that the NDI radical anions that form under reducing conditions enable attractive NDI–NDI interactions possibly due to charge delocalization between stacked NDI residues. This cyclic peptide system is considerably more complex than our simple NDI-Phe conjugates. In addition to putative NDI interactions, the cyclic peptide is also stabilized by formation of an extensive hydrogen bond network. Our NDI-Phe conjugates most likely assemble into structures that are primarily mediated by aromatic effects. Since our NDI conjugate **1b** has such a low molecular weight relative to Ghadiri's cyclic peptides, the effect of introducing negative charge to **1b** most likely results in a dominating repulsive effect that destabilizes the one-dimensional fibrils in favour of globular aggregates in which repulsive effects are presumably minimized.

We next analysed the nature of the reduced NDI species that exist upon addition of sodium dithionite in order to confirm formation of radical anions. We confirmed the formation of NDI radicals in our system by EPR spectroscopy (electronic supplementary material, figures S15–S17). We analysed both compounds **1a** and **1b** under conditions in which both were soluble and unassembled in order to simplify the measurements and also to confirm that formation of radical anions alone does not promote assembly of **1b**. Under oxidizing conditions, compounds **1a** and **1b** do not display any EPR signal (diamagnetic). In the presence of chemical reductant, however, both congeners display a characteristic EPR pattern at 298 K that is consistent with radical formation. The isotropic EPR spectra of **1a** and **1b** in aqueous solutions were obtained using a narrow magnetic field sweep width of 20 G. Both **1a** and **1b** showed similar EPR spectra (electronic supplementary material, figures S16 and S17, respectively) with 13 lines centred on a free radical *g*-value of 2.0, indicating free radical formation in both species. Owing to the hyperfine coupling, the main EPR transition of the radical anion is split into two equivalent nitrogen nuclei (^{14}N, $I = 1$; $a_N = 1.0$ G or $1.0 \times$

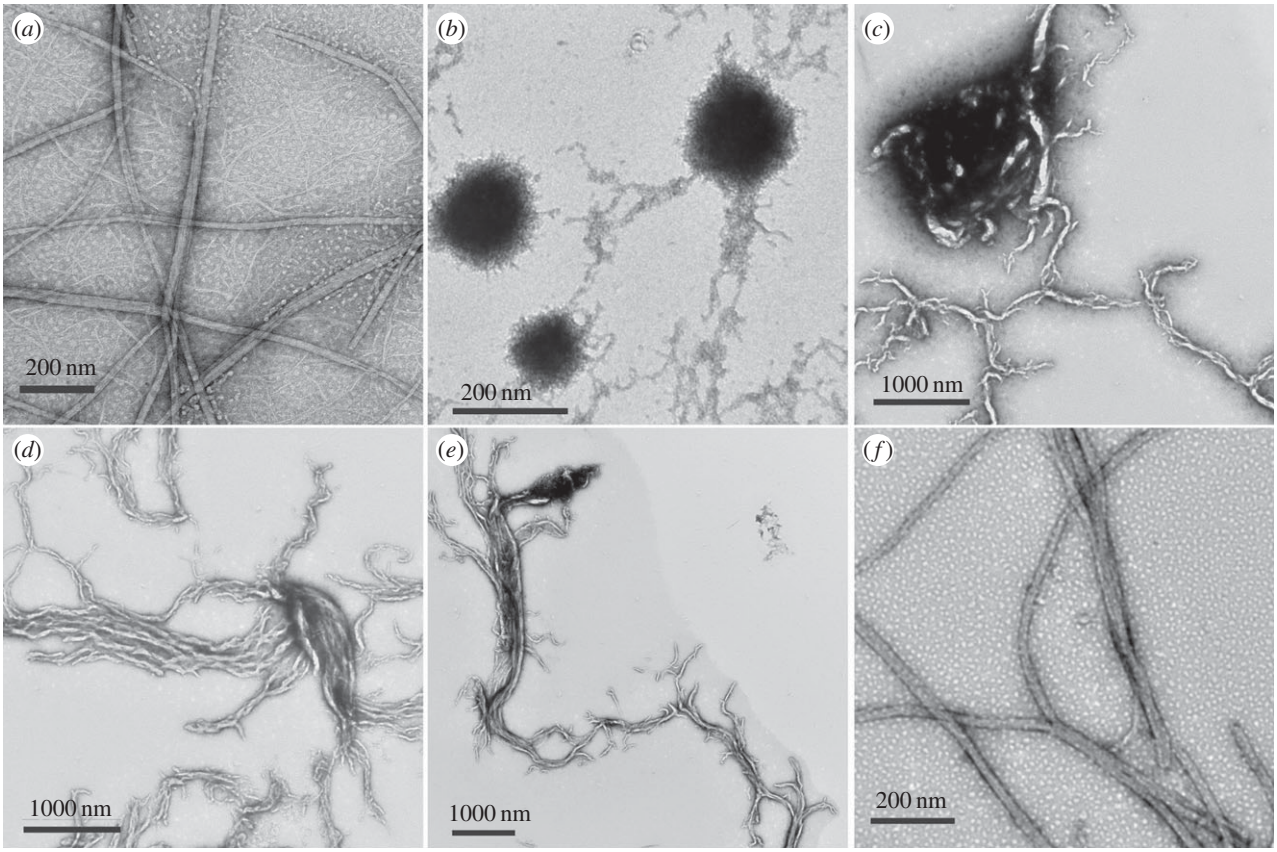

Figure 3. TEM images demonstrating the effects of reducing agents on the self-assembled fibril of compound **1b**. (*a*) Fibrils of **1b** (5 mM **1b**, 1 M NaCl) under ambient oxidizing conditions. (*b*) Fibrils of **1b** immediately after reduction by addition of $Na_2S_2O_4$ show loss of fibril morphology, replaced by irregular spherical aggregates. (*c–f*) Reduced **1b** aggregates 5 min (*c*), 30 min (*d*), 1 h (*e*) and 16 h (*f*) after addition of $Na_2S_2O_4$. Over this time frame, atmospheric oxygen re-establishes an oxidizing environment, facilitating complete reformation of the initially observed fibrils.

10^{-4} cm^{-1}), giving a 5-line spectrum. This is further split by four equivalent aromatic protons (^1H, $I = 1/2$; $a_H = 2.0$ G or 2.0×10^{-4} cm^{-1}) giving the resulting 13 lines. Small splitting from the two equivalent side chain CH protons is not resolved in either of the **1a** or **1b** EPR spectra. The larger line width seen in the **1b** EPR spectra may be attributed to further unresolved hyperfine splitting from fluorine nuclei. The *g*-values and hyperfine couplings are shown in electronic supplementary material, table S1. Taken together, these data indicate the formation of a free radical located on the NDI ring.

The redox properties of both **1a** and **1b** were further characterized using electrochemical methods. CV of these congeners was recorded in acetonitrile/water (1 : 1) with tetra-*N*-butylammonium perchlorate (TBAPC) as the supporting electrolyte (figure 4). Both **1a** and **1b** exhibited two well-separated reversible one-electron reduction processes, which are characteristic of sequential reduction of NDI to the mono radical anion ($NDI^{\bullet -}$) and dianion (NDI^{2-}) species. The anion radical was stable in anaerobic environments and compounds **1a** and **1b** regained their original molecular properties upon exposure to oxidizing conditions. The reduction and oxidation of these species could be repeated over many cycles (electronic supplementary material, figure S18) consistent with our observation that the morphological switching of aggregates of **1b** is repeatable.

Despite the observed differences in self-assembly propensity, both NDI-Phe congeners **1a** and **1b** possess similar typical photochemical behaviour under reducing conditions. UV–visible (UV–Vis) spectra of **1a** and **1b** were recorded in unbuffered H_2O (200 µmol), in the presence of chemical reductant (50 mM $Na_2S_2O_4$), and in the reoxidized state after addition of air/O_2 (figure 5). In native state, the spectra of both **1a** and **1b** exhibit two prominent absorption peaks at approximately 360 nm and 390 nm indicative of NDI $\pi-\pi^*$ transition polarized along the *Z*-axis of the NDI chromophore [31]. In the presence of $Na_2S_2O_4$, chemically reduced **1a** and **1b** peaks shifted to the visible region (λ_{max} approx. 454 nm and 476 nm, respectively), consistent with formation of radical anions [46]. However, in the presence of air/O_2 the peaks shifted back to near UV region (λ_{max} approx. 360 nm, 390 nm), confirming reoxidation of these species over time in ambient air.

The fluorescence emission spectra of **1a** and **1b** in the reduced state were analysed (figure 6). Spectra were collected at excitation wavelength of 476 nm. The fluorescence spectra from **1a** and **1b** in the reduced state show intense emission maxima (λ_{ex}) at 616 nm with a low energy shoulder at 660 nm (figure 6*a*). The red-shifted fluorescence emission is indicative of NDI aggregation in the reduced state. The fluorescence quantum yields of **1a** and **1b** were measured with fluorescein as a standard ($\Phi_{\mathbf{1a}} = 0.001$ and $\Phi_{\mathbf{1b}} = 0.023$, respectively) [47]. The low quantum yields obtained for these congeners are consistent with typical *N*-substituted NDI containing dyes [48,49], in which the decrease in fluorescence quantum yield may be due to strong hydrophobic interactions in water. However, in the presence of O_2/air, fluorescence intensity gradually decreased upon reoxidation to the native state.

As a whole, the EPR, CV and UV–Vis data described herein are consistent with previously reported data on similar NDI compounds [37,46,50–52]. These data suggest the formation

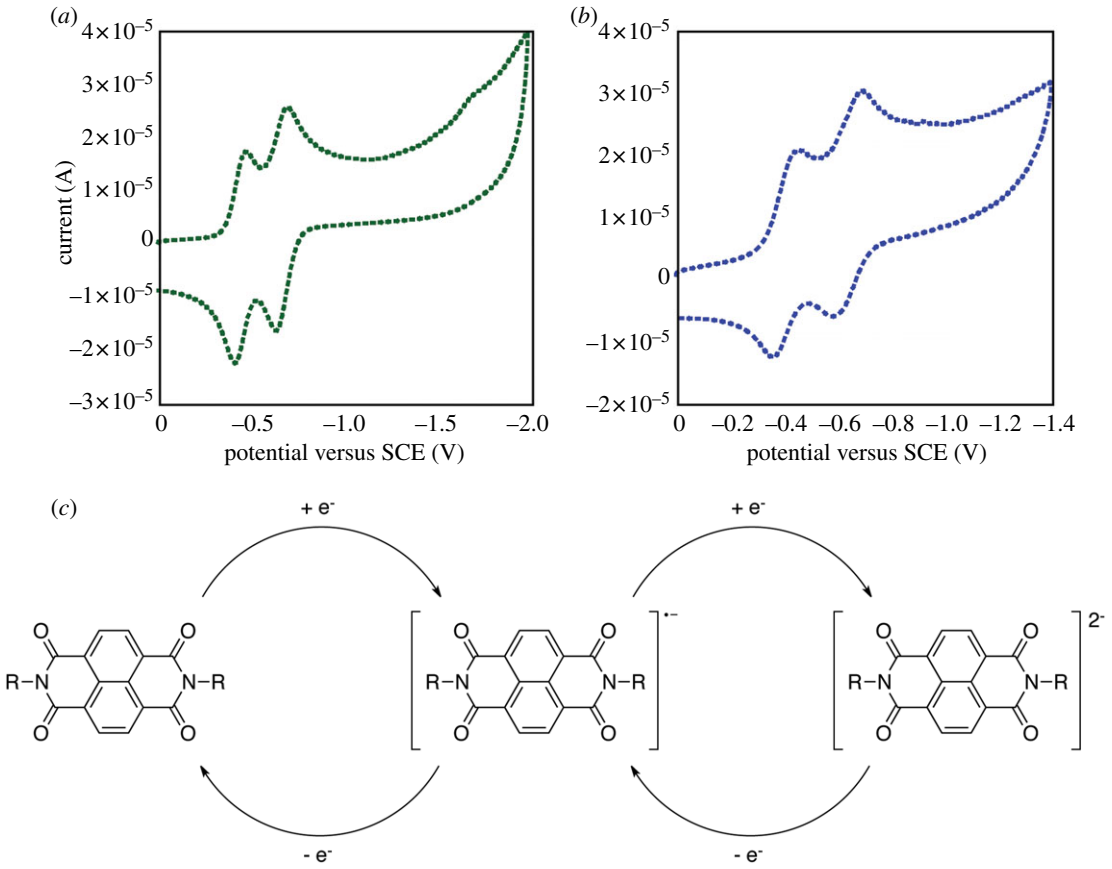

Figure 4. Cyclic voltammetry analysis of Phe-NDI conjugates in acetonitrile/H_2O (1 : 1). Tetra-*N*-butylammonium perchlorate is used as the supporting electrolyte; experiments were performed at 20°C with a glassy-carbon working electrode at a scan rate of 200 mV s^{-1}. (*a*) Cyclic voltammagram of compound **1a**, (*b*) cyclic voltammagram of compound **1b**. (*c*) A schematic of the reduction and reoxidation processes of NDI conjugates.

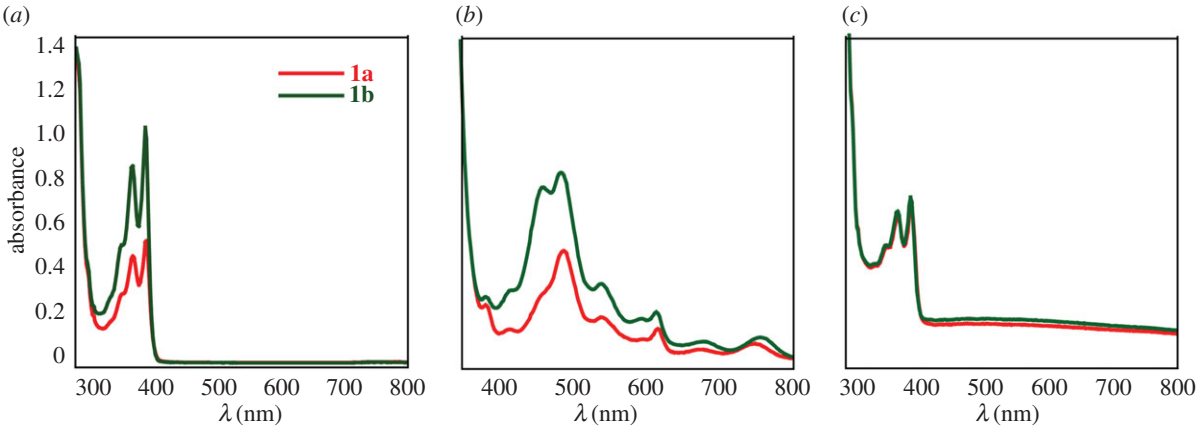

Figure 5. UV–Vis spectra of compounds **1a** and **1b** (*a*) in the native oxidized state, (*b*) in the reduced state after addition of sodium dithionite and (*c*) in the reoxidized state.

of a radical anion and dianion species, which results in the degradation of fibrils and formation of large aggregates upon reduction. It is significant that **1a** and **1b** have similar redox properties, but that only **1b** assembles into fibrils. This affirms the importance of hydrophobicity as a critical driving force in supramolecular assembly processes. It is also possible that the electron-deficient fluorinated benzene side chain the F_5-Phe conjugates mediates a unique intermolecular $\pi-\pi$ effect, accounting for this distinctive assembly behaviour. It also confirms that the self-assembly behaviour of these NDI-Phe conjugates under oxidizing conditions is independent of the redox potential of these molecules.

Precise structural insight into the self-assembled fibrils and globules of **1b** is impossible to derive from the data reported herein. Analysis of supramolecular structure of peptide and amino acid-based self-assemblies is often initiated using low resolution spectroscopic techniques such as CD and infrared spectroscopy. While these techniques are useful in providing clues about peptide secondary structure and, in some cases, other intermolecular interactions such as $\pi-\pi$ effects, they do

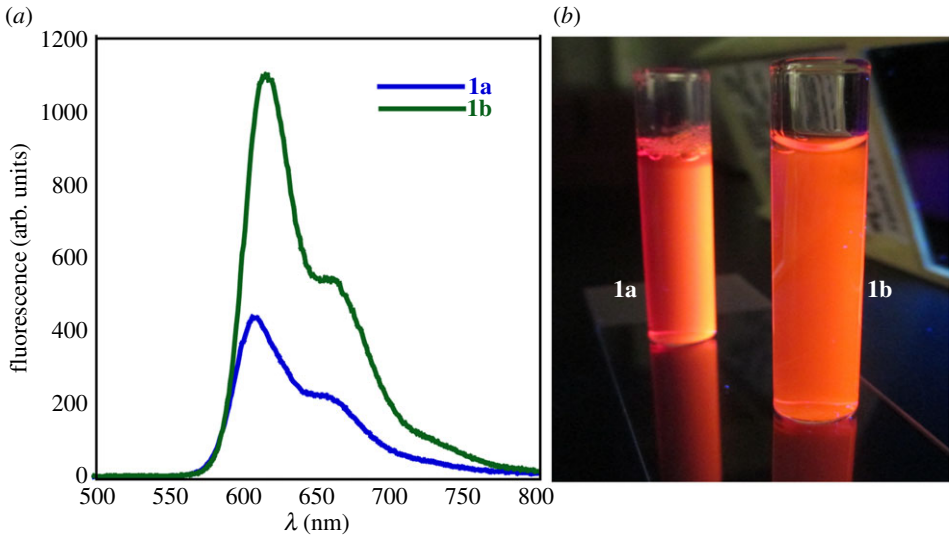

Figure 6. (*a*) Fluorescence emission spectra of reduced **1a** and **1b** (187 µmol) excited at 476 nm (fluorescence was detected at 616 nm); (*b*) digital images showing the fluorescence of reduced solutions of **1a** and **1b**.

not provide data of sufficient resolution to build strong packing models of supramolecular structures. To better understand the driving forces of self-assembly, X-ray crystal diffraction can be used. Unfortunately, materials that assemble into high-aspect ratio fibrils are notoriously difficult to crystallize. We were, however, able to obtain high-resolution crystal analyses of several of our synthetic intermediates (compounds **2a**, **3a** and **3b**; see electronic supplementary material, figures S19–S21 and appendices S1–S3). It is tempting to use these structural data to infer models of the self-assembled fibrils of **1b**, but we have opted to avoid this temptation. The crystals of these synthetic intermediates were formed in organic solvents that do not accurately reflect the environment of **1b** fibril assembly. In addition, these synthetic intermediates lack charge and, in the case of compounds **3a** and **3b**, include bulky Boc protecting groups on the amine functionality. As such, we suspect, based on the CD data, that intermolecular Phe side chain-side chain interactions occur. We also suspect that NDI–NDI interactions occur based on the morphological changes observed in the aggregates upon radical ion formation. However, we currently resist the proposal of a fibril packing model in the absence of high-resolution data that pertain directly to compound **1b** in water.

While the packing mode of the fibrils of **1b** remains unresolved, it is likely that the dramatic change in morphology that occurs upon reduction of the NDI moieties enforces a structural rearrangement that is more tolerant of intermolecular interactions that arise as a function of the negative charge on NDI in the reduced state. While it is premature to assign a distinct structure to the aggregates observed herein, their packing may be related to previously reported NDI–peptide or amino acid aggregates in which side chains stabilize NDI residues and allow for NDI stabilization [9,19,31,37,53]. Without high-resolution information regarding packing architecture in these aggregates, a detailed understanding of the mechanism(s) at play in the morphological transformations that are observed as a function of varying redox conditions is purely speculative. It is possible that NDI–NDI interactions occur in fibrils, which are then disrupted by Coulombic repulsion upon formation of radical anions under reducing conditions. Upon reoxidation, these repulsive effects are eliminated, enabling reorganization in the fibril packing mode. The ability to control the morphology of these NDI-Phe aggregates via a reductive trigger provides a useful template for future developments in supramolecular materials that respond dynamically to the environment.

4. Conclusion

Herein we report the stimulus-responsive morphological switching of supramolecular NDI-Phe aggregates in water. The superior self-assembly propensity of NDI-Phe conjugate **1b** can be attributed to the greater hydrophobicity of **1b** as well as the unique electron-deficient nature of the F_5-Phe side chain, reaffirming the critical nature of hydrophobic and aromatic effects in supramolecular self-assembly of low molecular weight peptides and amino acid derivatives. The observation of repeatable morphological shifting from supramolecular one-dimensional nanofibrils under oxidizing conditions to globular 100–200 nm aggregates with altered photophysical properties under reducing conditions is a dramatic demonstration of a material that responds dynamically to changes in the environment. These observations indicate the great potential of NDI/peptide-based materials for the creation of dynamic and responsive supramolecular architectures.

Authors' contributions. W.L. designed and carried out synthesis of materials and performed CD, UV–Vis, CV, EPR, NMR, TEM, SEM and self-assembly experiments. She also helped to draft the manuscript. P.W.R. supplemented W.L.'s synthetic and self-assembly work and assisted in drafting the manuscript. B.L.N. provided materials for experiments, helped with planning and designing of experiments and assisted in drafting of the manuscript. All authors gave final approval for publication.

Competing interests. We declare we have no competing interests.

Funding. This work was supported by the NSF (DMR-1148836).

Acknowledgements. We gratefully acknowledge Karen Bentley (University of Rochester Electron Microscopy Core) for her assistance with TEM imaging, Dr Scott Kennedy (University of Rochester) for assistance with CD experiments, Sandip Sur (University of Rochester) for assistance with EPR experiments, and Dr William Brennessel (University of Rochester) for assistance with XRD experiments.

References

1. Hirst AR, Escuder B, Miravet JF, Smith DK. 2008 High-tech applications of self-assembling supramolecular nanostructured gel-phase materials: from regenerative medicine to electronic devices. *Angew. Chem. Int. Ed.* **47**, 8002–8018. (doi:10.1002/anie.200800022)
2. Gao Y, Zhao F, Wang Q, Zhang Y, Xu B. 2010 Small peptide nanofibers as the matrices of molecular hydrogels for mimicking enzymes and enhancing the activity of enzymes. *Chem. Soc. Rev.* **39**, 3425–3433. (doi:10.1039/B919450A)
3. Zhao F, Ma ML, Xu B. 2009 Molecular hydrogels of therapeutic agents. *Chem. Soc. Rev.* **38**, 883–891. (doi:10.1039/B806410P)
4. Xu B. 2009 Gels as functional nanomaterials for biology and medicine. *Langmuir* **25**, 8375–8377. (doi:10.1021/la900987r)
5. Du X, Zhou J, Shi J, Xu B. 2015 Supramolecular hydrogelators and hydrogels: from soft matter to molecular biomaterials. *Chem. Rev.* **115**, 13 165–13 307. (doi:10.1021/acs.chemrev.5b00299)
6. Luo Q, Hou C, Bai Y, Wang R, Liu J. 2016 Protein assembly: versatile approaches to construct highly ordered nanostructures. *Chem. Rev.* **116**, 13 571–13 632. (doi:10.1021/acs.chemrev.6b00228)
7. Hauser CAE, Maurer-Stroh S, Martins IC. 2014 Amyloid-based nanosensors and nanodevices. *Chem. Soc. Rev.* **43**, 5326–5345. (doi:10.1039/C4CS00082J)
8. Bowerman CJ, Nilsson BL. 2012 Self-assembly of amphipathic β-sheet peptides: insights and applications. *Biopolymers* **98**, 169–184. (doi:10.1002/bip.22058)
9. Tovar JD. 2013 Supramolecular construction of optoelectronic biomaterials. *Acc. Chem. Res.* **46**, 1527–1537. (doi:10.1021/ar3002969)
10. Hirst AR, Smith DK. 2005 Two-component gel-phase materials—highly tunable self-assembling systems. *Chem. Eur. J.* **11**, 5496–5508. (doi:10.1002/chem.200500241)
11. Hirst AR, Miravet JF, Escuder B, Noirez L, Castelletto V, Hamley IW, Smith DK. 2009 Self-assembly of two-component gels: stoichiometric control and component selection. *Chem. Eur. J.* **15**, 372–379. (doi:10.1002/chem.200801475)
12. Hanabusa K, Miki T, Taguchi Y, Koyama T, Shirai H. 1993 Two-component, small molecule gelling agents. *J. Chem. Soc. Chem. Commun.* 1382–1384. (doi:10.1039/C39930001382)
13. Zelzer M, Todd SJ, Hirst AR, McDonald TO, Ulijn RV. 2013 Enzyme responsive materials: design strategies and future developments. *Biomater. Sci.* **1**, 11–39. (doi:10.1039/C2BM00041E)
14. Li X, Gao Y, Kuang Y, Xu B. 2010 Enzymatic formation of a photoresponsive supramolecular hydrogel. *Chem. Commun.* **46**, 5364–5366. (doi:10.1039/C0CC00163E)
15. Zhang Y, Zhang B, Kuang Y, Gao Y, Shi J, Zhang XX, Xu B. 2013 A redox responsive, fluorescent supramolecular metallohydrogel consists of nanofibers with single-molecule width. *J. Am. Chem. Soc.* **135**, 5008–5011. (doi:10.1021/ja402490j)
16. Ozbas B, Kretsinger J, Rajagopal K, Schneider JP, Pochan DJ. 2004 Salt-triggered peptide folding and consequent self-assembly into hydrogels with tunable modulus. *Macromolecules* **37**, 7331–7337. (doi:10.1021/ma0491762)
17. Schneider JP, Pochan DJ, Ozbas B, Rajagopal K, Pakstis L, Kretsinger J. 2002 Responsive hydrogels from the intramolecular folding and self-assembly of a designed peptide. *J. Am. Chem. Soc.* **124**, 15 030–15 037. (doi:10.1021/ja027993g)
18. Bhosale SV, Jani CH, Langford SJ. 2008 Chemistry of naphthalene diimides. *Chem. Soc. Rev.* **37**, 331–342. (doi:10.1039/B615857A)
19. Katz HE, Lovinger AJ, Johnson J, Kloc C, Slegrist T, Li W, Lin YY, Dodabalapur A. 2000 A soluble and air-stable organic semiconductor with high electron mobility. *Nature* **404**, 478–481. (doi:10.1038/35006603)
20. Kobaisi MA, Bhosale SV, Latham K, Raynor AM, Bhosale SV. 2016 Functional naphthalene diimides: synthesis, properties, and applications. *Chem. Rev.* **116**, 11 685–11 796. (doi:10.1021/acs.chemrev.6b00160)
21. Nalluri SKM, Liu Z, Wu Y, Hermann KR, Samanta A, Kim DJ, Krzyaniak MD, Wasielewski MR, Stoddart JF. 2016 Chiral redox-active isosceles triangles. *J. Am. Chem. Soc.* **138**, 5968–5977. (doi:10.1021/jacs.6b02086)
22. Schroot R, Schlotthauer T, Schubert US, Jäger M. 2016 Modular assembly of poly(naphthalene diimide) and Ru(II) dyes for an efficient light-induced charge separation in hierarchically controlled polymer architectures. *Macromolecules* **49**, 2112–2123. (doi:10.1021/acs.macromol.5b02717)
23. Chen M, Yang C, Xu Z, Tang Y, Jiang J, Liu P, Su Y, Wu D. 2016 A facile self-assembly strategy towards naphthalene diimide/graphene hybrids as high performance organic cathodes for lithium-ion batteries. *RSC Adv.* **6**, 13 666–13 669. (doi:10.1039/C5RA26181C)
24. Pandeeswar M, Khare H, Ramakumar S, Govindaraju T. 2015 Crystallographic insight-guided nanoarchitectonics and conductivity modulation of an n-type organic semiconductor through peptide conjugation. *Chem. Commun.* **51**, 8315–8318. (doi:10.1039/C5CC01996F)
25. Avinash MB, Govindaraju T. 2011 Engineering molecular organization of naphthalenediimides: large nanosheets with metallic conductivity and attoliter containers. *Adv. Funct. Mater.* **21**, 3875–3882. (doi:10.1002/adfm.201101001)
26. Avinash MB, Govindaraju T. 2011 A bio-inspired design strategy: organization of tryptophan-appended naphthalenediimide into well-defined architectures induced by molecular interactions. *Nanoscale* **3**, 2536–2543. (doi:10.1039/c0nr00766h)
27. Das A, Ghosh S. 2016 H-bonding directed programmed supramolecular assembly of naphthalene-diimide (NDI) derivatives. *Chem. Commun.* **52**, 6860–6872. (doi:10.1039/C6CC01983H)
28. Rananaware A, Samanta M, Bhosale RS, Kobaisi MA, Roy B, Bheemireddy V, Bhosale SV, Bandyopadhyay S, Bhosale SV. 2016 Photomodulation of fluoride ion binding through anion-π interactions using a photoswitchable azobenzene system. *Sci. Rep.* **6**, 22928. (doi:10.1038/srep22928)
29. Bhosale RS, Al Kobaisi M, Bhosale SV, Bhargava S, Bhosale SV. 2015 Flower-like supramolecular self-assembly of phosphonic acid appended naphthalene diimide and melamine. *Sci. Rep.* **5**, 14609. (doi:10.1038/srep14609)
30. Shao H, Nguyen T, Romano NC, Modarelli DA, Parquette JR. 2009 Self-assembly of 1-Dn-type nanostructures based on naphthalene diimide-appended dipeptides. *J. Am. Chem. Soc.* **131**, 16 374–16 376. (doi:10.1021/ja906377q)
31. Shao H, Parquette JR. 2010 A π-conjugated hydrogel based on an Fmoc-dipeptide naphthalene diimide semiconductor. *Chem. Commun.* **46**, 4285–4287. (doi:10.1039/C0CC00701C)
32. Nalluri SKM, Berdugo C, Javid N, Frederix PWJM, Ulijn RV. 2014 Biocatalytic self-assembly of supramolecular charge-transfer nanostructures based on n-type semiconductor-appended peptides. *Angew. Chem. Int. Ed.* **53**, 5882–5887. (doi:10.1002/anie.201311158)
33. Liu Y-H, Hsu S-M, Wu F-Y, Cheng H, Yeh M-Y, Lin H-C. 2014 Electroactive organic dye incorporating dipeptides in the formation of self-assembled nanofibrous hydrogels. *Bioconjugate Chem.* **25**, 1794–1800. (doi:10.1021/bc500299c)
34. Hsu L-H, Hsu S-M, Wu F-Y, Liu Y-H, Nelli SR, Yeh M-Y, Lin H-C. 2015 Nanofibrous hydrogels self-assembled from naphthalene diimide (NDI)/amino acid conjugates. *RSC Adv.* **5**, 20 410–20 413. (doi:10.1039/C5RA00172B)
35. Goskulwad SP, La DD, Bhosale RS, Al Kobaisi M, Bhosale SV, Bhosale SV. 2016 Golf ball-like architecture fabricated by supramolecular self-assembly of naphthalene diimide. *RSC Adv.* **6**, 39 392–39 395. (doi:10.1039/C6RA06927D)
36. Nandre KP, Bhosale SV, Rama Krishna, KVS, Gupta A, Bhosale SV. 2013 A phosphonic acid appended naphthalene diimide motif for self-assembly into tunable nanostructures through molecular recognition with arginine in water. *Chem. Commun.* **49**, 5444–5446. (doi:10.1039/C3CC41259H)
37. Ashkenasy N, Horne WS, Ghadiri MR. 2006 Design of self-assembling peptide nanotubes with delocalized electronic states. *Small* **2**, 99–102. (doi:10.1002/smll.200500252)
38. Tao K, Levin A, Adler-Abramovich L, Gazit E. 2016 Fmoc-modified amino acids and short peptides: simple bio-inspired building blocks for the fabrication of functional materials. *Chem. Soc. Rev.* **45**, 3935–3953. (doi:10.1039/C5CS00889A)

39. Ryan DM, Nilsson BL. 2012 Self-assembled amino acids and dipeptides as noncovalent hydrogels for tissue engineering. *Polym. Chem.* **3**, 18–33. (doi:10.1039/c1py00335f)
40. Ryan DM, Anderson SB, Nilsson BL. 2010 The influence of side-chain halogenation on the self-assembly and hydrogelation of Fmoc-phenylalanine derivatives. *Soft Matter* **6**, 3220–3231. (doi:10.1039/c0sm00018c)
41. Draper ER, Morris KL, Little MA, Raeburn J, Colquhoun C, Cross ER, McDonald TO, Serpell LC, Adams DJ. 2015 Hydrogels formed from Fmoc amino acids. *CrystEngComm* **17**, 8047–8057. (doi:10.1039/C5CE00801H)
42. Sutton S, Campbell NL, Cooper AI, Kirkland M, Frith WJ, Adams DJ. 2009 Controlled release from modified amino acid hydrogels governed by molecular size or network dynamics. *Langmuir* **25**, 10 285–10 291. (doi:10.1021/la9011058)
43. Ryan DM, Anderson SB, Senguen FT, Youngman RE, Nilsson BL. 2010 Self-assembly and hydrogelation promoted by F_5-phenylalanine. *Soft Matter* **6**, 475–479. (doi:10.1039/b916738b)
44. Andric G *et al.* 2004 Spectroscopy of naphthalene diimides and their anion radicals. *Aust. J. Chem.* **57**, 1011–1019. (doi:10.1071/CH04130)
45. Bowerman CJ, Liyanage W, Federation AJ, Nilsson BL. 2011 Tuning β-sheet peptide self-assembly and hydrogelation behavior by modification of sequence hydrophobicity and aromaticity. *Biomacromolecules* **12**, 2735–2745. (doi:10.1021/bm200510k)
46. Gosztola D, Niemczyk MP, Svec W, Lukas AS, Wasielewski MR. 2000 Excited doublet states of electrochemically generated aromatic imide and diimide radical anions. *J. Phys. Chem. A* **104**, 6545–6551. (doi:10.1021/jp000706f)
47. Hapuarachchige S *et al.* 2011 Design and synthesis of a new class of membrane-permeable triazaborolopyridinium fluorescent probes. *J. Am. Chem. Soc.* **133**, 6780–6790. (doi:10.1021/ja2005175)
48. Basak S, Nanda J, Banerjee A. 2013 Assembly of naphthalenediimide conjugated peptides: aggregation induced changes in fluorescence. *Chem. Commun.* **49**, 6891–6893. (doi:10.1039/C3CC43538E)
49. Würthner F, Kaiser TE, Saha-Möller CR. 2011 J-aggregates: from serendipitous discovery to supramolecular engineering of functional dye materials. *Angew. Chem. Int. Ed.* **50**, 3376–3410. (doi:10.1002/anie.201002307)
50. Ford WE, Hiratsuka H, Kamat PV. 1989 Photochemistry of 3,4,9,10-perylenetetracarboxylic dianhydride dyes. 4. Spectroscopic and redox properties of oxidized and reduced forms of the bis(2,5-di-tert-butylphenyl)imide derivative. *J. Phys. Chem.* **93**, 6692–6696. (doi:10.1021/j100355a025)
51. Viehbeck A, Goldberg MJ, Kovac CA. 1990 Electrochemical properties of polyimides and related imide compounds. *J. Electrochem. Soc.* **137**, 1460–1466. (doi:10.1149/1.2086690)
52. Lee SK, Zu Y, Herrmann A, Geerts Y, Muellen K, Bard AJ. 1999 Electrochemistry, spectroscopy and electrogenerated chemiluminescence of perylene, terrylene, and quaterrylene diimides in aprotic solution. *J. Am. Chem. Soc.* **121**, 3513–3520. (doi:10.1021/JA984188M)
53. Pengo P, Pantoş GD, Otto S, Sanders JKM. 2006 Efficient and mild microwave-assisted stepwise functionalization of naphthalenediimide with α-amino acids. *J. Org. Chem.* **71**, 7063–7066. (doi:10.1021/jo061195h)